IOP Publishing Mater. Res. Express 4 (2017) 046401 https://doi.org/10.1088/2053-1591/aa6953

Materials Research Express

RECEIVED
26 February 2017

REVISED
22 March 2017

ACCEPTED FOR PUBLICATION
27 March 2017

PUBLISHED
12 April 2017

PAPER

Effect of Ag and Ti electrodes on capacitance tunability of oxygen-deficient $SrTiO_3$ based MIM varactors prepared by plasma sputtering

Saqib Jabbar[1], R Ahmad[1], Chenxi Wang[2] and Paul K Chu[2]

[1] Government College University, Lahore 54000, Pakistan

[2] Department of Physics and Materials Science, City University of Hong Kong, Tat Chee Avenue, Kowloon, Hong Kong, People's Republic of China

E-mail: paul.chu@cityu.edu.hk **(Paul K Chu)**

Keywords: strontium titanate, tunability, quality factor, varactors

Abstract

The role of oxygen deficiencies on the electrical performance of $SrTiO_3$ films is investigated by depositing on the stack of $TiN/Ti/SiO_2/Si$ films using radio-frequency (RF) and direct current (DC) magnetron sputtering systems operating in oxygen-deficient plasma environment. Electrodes of silver (Ag) and titanium (Ti) are used to observe the effects of their sizes on the electrical properties of the $SrTiO_3$ films. It is found that the nonlinearity in capacitance–voltage graphs (capacitance tunability) of the varactor can be controlled by varying the electrode area. In addition, the material of the electrode plays a vital role in controlling the non-linearity in the capacitance of the oxygen-deficient $SrTiO_3$ dielectric films with varying voltage. It is found that the silver top electrode instead of titanium, delivers better performance with high capacitance tunability, low leakage current and good quality factor. Post deposition annealing at 550 °C in nitrogen ambient, creates more oxygen deficiencies in $SrTiO_3$ film thereby increasing the linearity of the capacitance–voltage graph and decreasing the capacitance tunability.

1. Introduction

High permittivity dielectric materials with field dependence permittivity have large application potential in radio-frequency (RF) circuits, microwave components, capacitors, transmission lines, resonators, and phase shifters due to their nonlinear capacitive behavior with respect to the applied voltage [1]. The parallel plate metal-insulator-metal (MIM) capacitor which has low fringing fields, high capacitance density, and low tuning voltage [2] is capped by voltage-tunable integrated capacitors (varactors). Varactors are widely used as continuously tunable capacitors due to their improved power handling and simpler biasing compared to diodes [3]. As there is no forward conduction region in varactors, they can sustain a large RF voltage swing especially near zero volts. The voltage control functionality can thus be devised with greater simplicity, efficiency, and robustness than the magnetic control device [4]. In comparison to micro-electromechanical systems (MEMS), they are physically smaller, require less processing, and have a fast intrinsic response time. The tunable components can decrease the dimensions of the electronic circuits by exploiting the re-configurability of the circuit [5]. In this respect, thin ferroelectric films are very attractive to tunable applications due to the small tuning bias, low production cost, as well as high integrability. Barium strontium titanate and strontium titanate (STO) have commercial applications on account of the high capacitance density [6, 7] and in particular STO films are cost effective and have a low processing temperature (500 °C) and high dielectric constant (max. 300) [8, 9]. STO has incipient ferroelectric properties. That is, on the one hand, its dielectric behavior is fully controlled by the soft mode dynamics [10] but on the other hand, it remains paraelectric down to the lowest temperature due to quantum fluctuations [11]. These unique properties render STO a good candidate in tunable RF/microwave components.

The dependence of nonlinearity in capacitance–voltage graphs for the $STO/TiN/Ti/SiO_2/Si$ structure on various parameters such as the electrode area, materials of the top electrode, and annealing have been investigated. The titanium nitride (TiN) thin film was deposited between titanium (Ti) and STO thin films to mitigate

© 2017 IOP Publishing Ltd

Table 1. Important deposition conditions.

Film	Ar flow rate (sccm)	Power (W)	Pressure (mTorr)	Time (min)	Deposition rate (Å s^{-1})	Thickness (nm)
SiO_2	15	200	4.0	40	0.21	50
Ti	10	150	3.0	12	0.69	50
TiN	5 (N_2 = 15)	200	3.0	20	0.42	50
STO	15	200	5.0	30	0.28	50

diffusion [12]. Silicon dioxide (SiO_2) film has been deposited to increase the resistivity of the substrate to minimize the leakage currents [13]. The electrode materials, size of the electrode, and annealing temperature played important role in the capacitance tunability (τ), capacitance density (C_d), quality factor (Q), and dielectric constant of the capacitor. Where τ and Q define the change in capacitance with applied dc bias and rate of energy losses relative to the stored energy of capacitor respectively. Other parameters such as the deposition method, film composition, thickness and area of the electrode also affected the performance of the STO thin film. Partial pressure of oxygen plays a vital role in generation of oxygen vacancies and STO films. STO films grown in low oxygen partial pressure have higher number of oxygen vacancies [14, 15]. In order to study the effects of oxygen vacancies, films have been sputter-deposited in an argon (Ar) atmosphere at a low base pressure of 1×10^{-7} Torr. The thickness of the STO insulator and the other films (SiO_2, TiN and Ti) was about 50 nm. The C–V and I–V results disclose a clear dependence on the oxygen deficiencies and thicker films were expected to result in worse tunability. This is because only the thin upper layer of the thick ferroelectrics contributes to effective tuning [14]. The surface morphology, crystallinity and roughness of the STO film strongly affected the K values [15]. That is why, the STO/TiN/Ti/SiO_2/Si structure was annealed at the crystallization temperature of STO (550 °C) to study the effect of crystallinity. Extensive use of platinum and ruthenium dioxide as metal electrodes to avoid oxidation due to their high conductivities and work function, raised the manufacturing cost [15]. Therefore, it is needed to identify less expensive materials with large work functions. In this respect, almost all of the previously reported devices suffer from the same limitation that the value of τ on the single wafer is the same [16]. Herein, to overcome this limitation, we describe a new area-variable varactor with τ being a function of the top electrode area. Our results also show that by selecting the proper electrode size and materials, the electrical properties of the capacitor can be tuned.

2. Experimental details

P-type Si (1 0 0) samples with dimensions of $1.5 \times 1.5\ cm^2$ were used as substrates. The samples were cleaned with acetone, methanol, and deionized water sequentially for 15 min each in an ultrasonic bath. The AJA ATC ORION magnetron sputtering system with five targets was used to deposit the thin films. The system was equipped with direct current (DC) and RF (13.56 MHz) power supplies as well as *in situ* substrate heating, rotation and thickness measurement arrangements. The optimal deposition conditions were determined before deposition by measuring the deposition rates of all the films with the MCM-160 rate/thickness meter with the shutter at closed position. The distance of sample holder from the target and its rate of rotation were fixed at 10 cm and 50 rev min^{-1} respectively. The chamber was evacuated to a base pressure of 1×10^{-7} Torr and the films were deposited at room temperature. The important deposition conditions are provided in table 1. RF was used to deposit the SiO_2 and STO thin films whereas DC was employed to deposit the Ti and TiN films. Only argon gas was used as a sputtering gas to produce the oxygen deficient STO films in an oxygen deficient environment. After deposition, some of the samples were annealed *in situ* at 550 °C for 10 min in nitrogen (flow rate of 10 sccm and pressure of 4×10^{-4} Torr). Masks with circular holes of areas A1, A2, A3, A4 and A5 approximately equal to 7.9×10^{-3}, 3.1×10^{-2}, 4.3×10^{-2}, 5.6×10^{-2}, and $8.7 \times 10^{-2}\ mm^2$ respectively were used to sputter deposit the Ag and Ti electrodes. The top electrodes were deposited on to the stacked structure after annealing to avoid the diffusion of the electrode material into the STO film at high temperature generating the hybrid structure [17, 18]. Structural and morphological properties were studied by using D2 Phaser x-ray diffractometer using Cu-K_α radiations and FEI Quanta 450 FESEM system. The electrical properties of the capacitors are studied by using Keithley 4200 SCS system.

3. Results and discussion

Figure 1(a) shows the x-ray diffraction (XRD) graph of the as-deposited and annealed stacked MIM structure. Before annealing, the STO film is almost amorphous with the exception of the (0 0 1 2) reflection with a high signal-to-noise ratio [19]. Lukosius *et al* [20] also observed that STO films deposited on TiN may be crystalline and a sharp

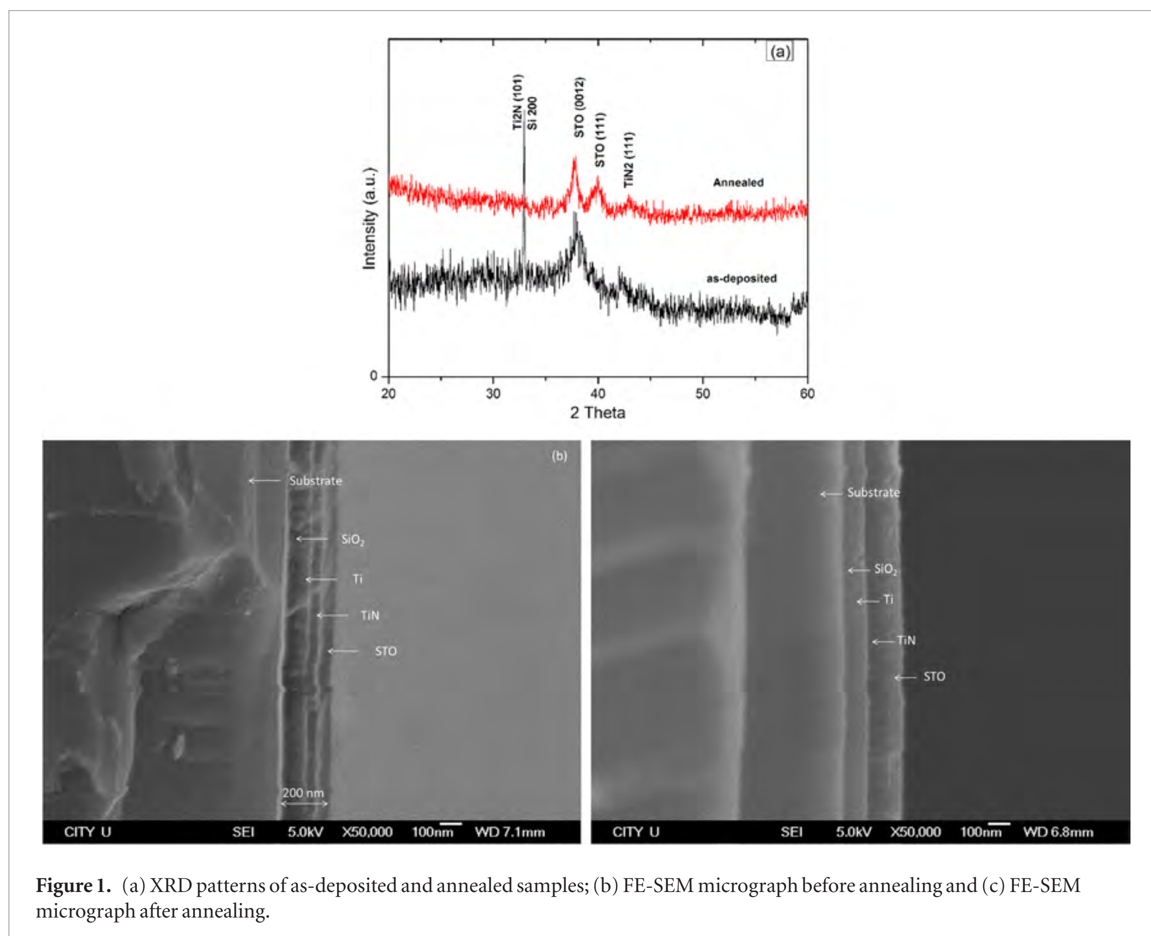

Figure 1. (a) XRD patterns of as-deposited and annealed samples; (b) FE-SEM micrograph before annealing and (c) FE-SEM micrograph after annealing.

peak at about 33° indicates the Ti_2N phase with (1 0 1) reflection [21]. This is due to the small nitrogen content in the plasma. After annealing, the Ti_2N phase vanishes and the TiN phase becomes more dominant due to the larger nitrogen concentration at the high annealing temperature [22]. The STO (0 0 1 2) peak becomes prominent and a new STO (1 1 1) peak emerges indicative of a more structured form.

Figures 1(b) and (c) show the cross-sectional field emission scanning electron microscope (FE-SEM) micrographs of the as-deposited and annealed samples, respectively. Although the images are not very sharp due to the insulating nature of the SiO_2 and STO films, the stacked/layered structure is clearly observed. The total thickness of all the films is found to be around 200 nm and it is consistent with the measurement made by the thickness meter. After annealing, uniform layers are observed providing clear information about the film structure.

The capacitance is measured at 1 MHz frequency and 20 mV AC was used to minimize errors arising from the nonlinear properties of varactors. Figure 2(a) shows the *C*–*V* curve of the MIM varactors with Ag top electrodes of different areas from A1 to A5. With regard to small top electrode areas such as A1 and A2, the *C*–*V* curves are almost straight and symmetrical around 0 V and the capacitance increases from 1.2×10^{-10} to 4.7×10^{-10} F. As the area is increased more than A2, the capacitance around 0 V goes up and the curves become more nonlinear. At certain processing conditions space-charge can buildup near the electrode due to the migration of charged defects such as oxygen deficiencies. The internal field of these charged deficiencies interacts with the applied field which can vary the linearity of the capacitance. The amount of oxygen deficiencies increases with increasing the area and capacitors with small areas show lesser nonlinearity as compared to the larger ones on the same wafer. The gradually changing (not abrupt) *C*–*V* curves for A1 and A2 indicate that the concentration of oxygen deficiencies is uniform under the electrode area, and the capacitance is increasing by increasing the area near 0 V. On increasing the area more than A2, we can see some abrupt changes in the curves for high voltages ($-1 > V > 1$) and the capacitance is decreasing at about −3 V. These changes are attributed to the field fringing effect (FFE) at the electrode periphery. Fringing field has the effect on capacitance to increase and, consequently, the electrostatic force would also increase [23]. It can be seen that at −3 V, the capacitance is decreasing by increasing the area larger than A2 but, it is increasing correspondingly near 0 V with the size of electrode. This indicates the FFE is higher for small areas A1 and A2 and for large areas it has almost negligible effects for high voltages. It has also been reported that high electric field at the electrode edges reduces the permittivity, and the fringing capacitance can be tuned with bias voltage. It should have negligible impact on the tunability curve, other than to increase the total capacitance [24]. For A5, capacitance starts to increase at −3 V but still its value is much lower than A2. After the reversal of the applied field a small increase in the capacitance towards positive voltage is stemmed from incomplete removal

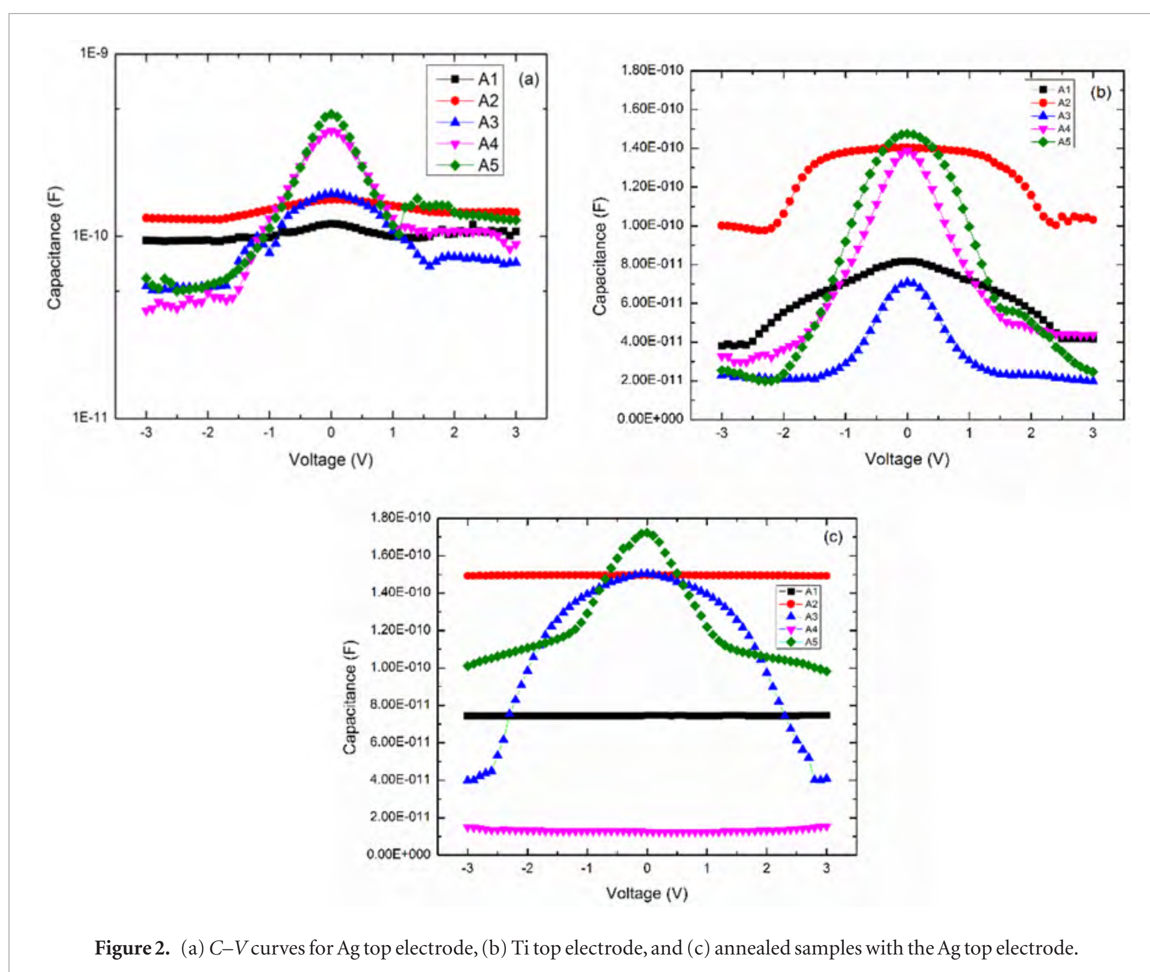

Figure 2. (a) C–V curves for Ag top electrode, (b) Ti top electrode, and (c) annealed samples with the Ag top electrode.

of the positively charged oxygen deficiencies. A significant change in the trend of the curve by increasing the area from A3 can be observed. This trend change can be observed in all the C–V curves measured for both Ag and Ti electrodes by increasing the electrode area greater than A3 and capacitance becomes more nonlinear with varying voltage.

Figure 2(b) shows that by using the Ti electrodes, the capacitance decreases about 10 times than is achieved by Ag electrodes with the same sizes. The lower work function of Ti (4.3 eV) as compared to Ag (5.1 eV) increases the possibility of forming the heterostuctures at the interface under the electrode area. The graphs are showing the same trend for Ti as for Ag electrodes and their nonlinearity is increasing by increasing the area. The increase in nonlinearity is attributed to the higher number of oxygen deficiencies under the Ti electrodes due to lower work function than Ag. Oxygen deficiencies decrease the attractive Coulomb forces between the nearest cation and anion atoms thereby increasing the lattice parameter and nonlinearity [12]. Electrical resistivity of Ti (43×10^{-8} Ω m) is higher as compared to Ag (1.59×10^{-8} Ω m) which can enhance the effect of series resistance between top and bottom electrode at high frequency of 1 MHz. The effect of series resistance can be minimized by making the electrode sizes smaller and thicker. FFE can also be observed here and are showing approximately the same trend as for Ag electrodes at -3 V.

After annealing the samples and deposition of Ag electrodes, straight lines are obtained for A1 and A2 as shown in figure 2(c). For A4, C–V curve shows a different trend having small positive voltage coefficient of capacitance (V_{cc}) every time after repeating the voltage sweep. It has been reported that crystalline STO is paraelectric displaying negative value of V_{cc} [25] but positive V_{cc} has also been reported [20, 26, 27]. In the XRD patterns, although the signal-to-noise ratio improves after annealing, the peak intensity of STO (1 1 1) is quite low showing that 10 min are not sufficient to achieve complete crystallinity and to recover the equilibrium oxygen stoichiometry [28]. The positive response is due to lower and non uniform crystallinity, and oxygen deficiencies controlling the nonlinearity of the STO film under A4 [14]. According to Szot *et al* [29] this may be due to the localized decomposition and subsequent accumulation of oxygen gas by the preferential diffusion of oxygen and solid state electrolytic processes under the electrode which is highly probable due to non uniform crystallinity. That is why only A4 is showing the different C–V behavior. Hence, by increasing the area, the concentration of oxygen vacancy decreases and C–V curves show negative V_{cc}. For the area A5, the curve is again nonlinear at higher negative V_{cc}. We can see that at -3 V, it has the same trend of changing the capacitance as observed for un-annealed structures as discussed earlier. Results suggest that the linearity of the STO-based varactors depends on the annealing temperature, size

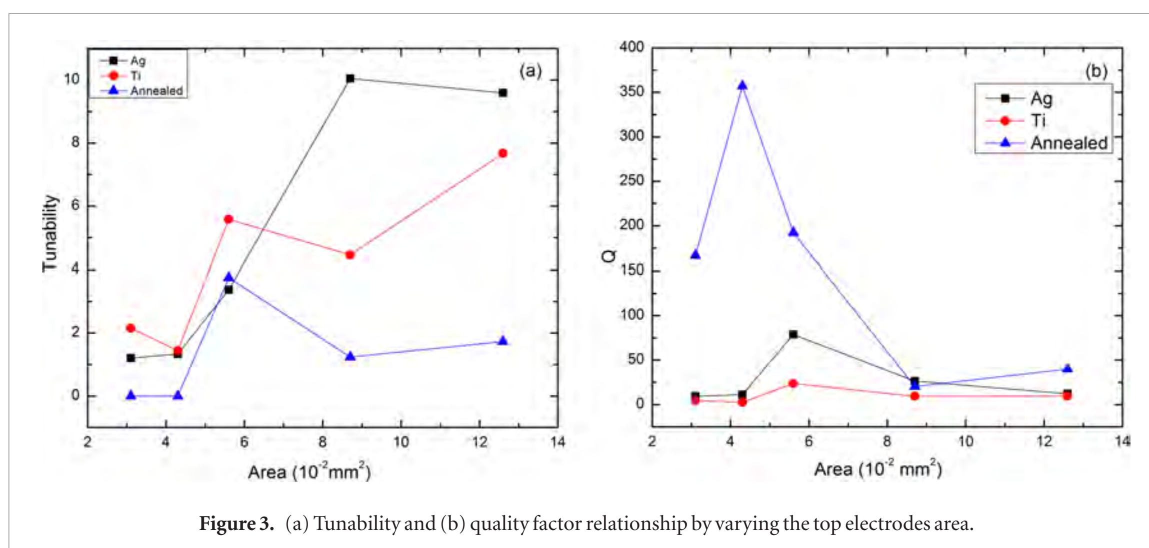

Figure 3. (a) Tunability and (b) quality factor relationship by varying the top electrodes area.

as well as material of the top electrode. For areas lesser than A3, C–V curves have negligible variations and become straight after annealing.

The τ is calculated by the following formula [12]:

$$\tau = C_{\max}/C_{\min},$$

where $C_{\max}$ is the capacitance at 0 V and $C_{\min}$ is the minimum value of the capacitance. The results are consistent with previous data that τ increases with larger area [20]. In the low voltage range of ± 3 V, large τ values are observed. Figure 3(a) shows the dependence of the τ on the Ag and Ti top electrode areas for the as-deposited and annealed films. For the Ag electrodes, τ increases by increasing the area. For A1 and A2, the value is small (<1.5) but increasing the area to A4 raises it to 10.0 followed by a small decrease to 9.6. With regard to the Ti electrodes, τ increases with the area but the values are smaller (maximum 7.67 for A5). After annealing, the same trend is observed from the Ag electrodes but with lower τ (maximum 3.75 for A3). This is because the C–V curves become more linear after annealing.

The Q is also calculated by the following formula:

$$Q = 1/D = 2\pi fC/G,$$

Where D is the dissipation factor, G is the conductance, f is the frequency, and C is the capacitance of the capacitor. Q is calculated at 0 V and plotted against the electrode area in figure 3(b). Devices in real applications have high trade-offs between Q and τ [5]. For the area A4, τ has the maximum value of 10.05 but the quality factor Q is very low (25.5). In comparison, Q reaches the maximum value of 357.9 for the annealed sample with area A2 and τ is almost zero. Similarly, for annealed A3, Q is high up to 192.4, but τ is only about 1.17. The tuning range of a given diode can be traded for the quality factor if only a part of the tuning range is used. Kim *et al* [16] have proposed that the change in τ of the varactors on the single wafer is due to the change in the effective depletion area under the electrodes. Accordingly, for 0 V, the effective depletion area is large and becomes very small when it is fully reverse biased. This is because that the depletion regions under the floating contacts are isolated from the depletion region under the cathode giving rise to large τ values which are proportional to the area ratio of the floating contacts. Very low values of Q for Ti electrodes are due to the effect of series resistance which causes dielectric losses.

Figure 4 depicts the I–V characteristics of the varactors. The Ag top electrode on the as-deposited film in figure 4(a) shows asymmetric I–V curves. During negative to positive biasing, the current decreases first and smoothly reaches a minimum at some negative voltage, and then increases. The leakage currents may originate from either Schottky emission (SE) or Poole–Frenkel emission (PFE) [30, 31]. SE arises from the materials-electrode interface and PFE is due to the bulk properties of the insulator. In case of PFE, oxygen vacancies act as internal traps in the bulk [32]. Comparing the I–V curves in figure 4, it can be concluded that the leakage current stems from both types of emissions. The A1 electrode shows that it decreases linearly from -3 V to -2.5 V, drops to the lowest leakage current value at -1.6 V, and then increases linearly again from -1 V to 3 V but with a larger slope. The fixed positive charges at the STO/TiN interface give rise to the internal electric field which combines with the applied field [33]. These fixed charges repel the positively-charged oxygen vacancies and increase the distance between them and the electrode. The direction of the current induced by the applied field is opposite to the direction which would be generated by the fixed charges at a low negative bias. This is why a thicker barrier and larger bias are required to saturate the tunneling injection of carriers into the oxide film [33, 34]. Figure 4(a) shows that the minimum in the leakage current is in the negative bias region. When a positive bias is applied, the oxygen vacancies are repelled towards the bottom electrode to enhance electron injection and increase the leakage current.

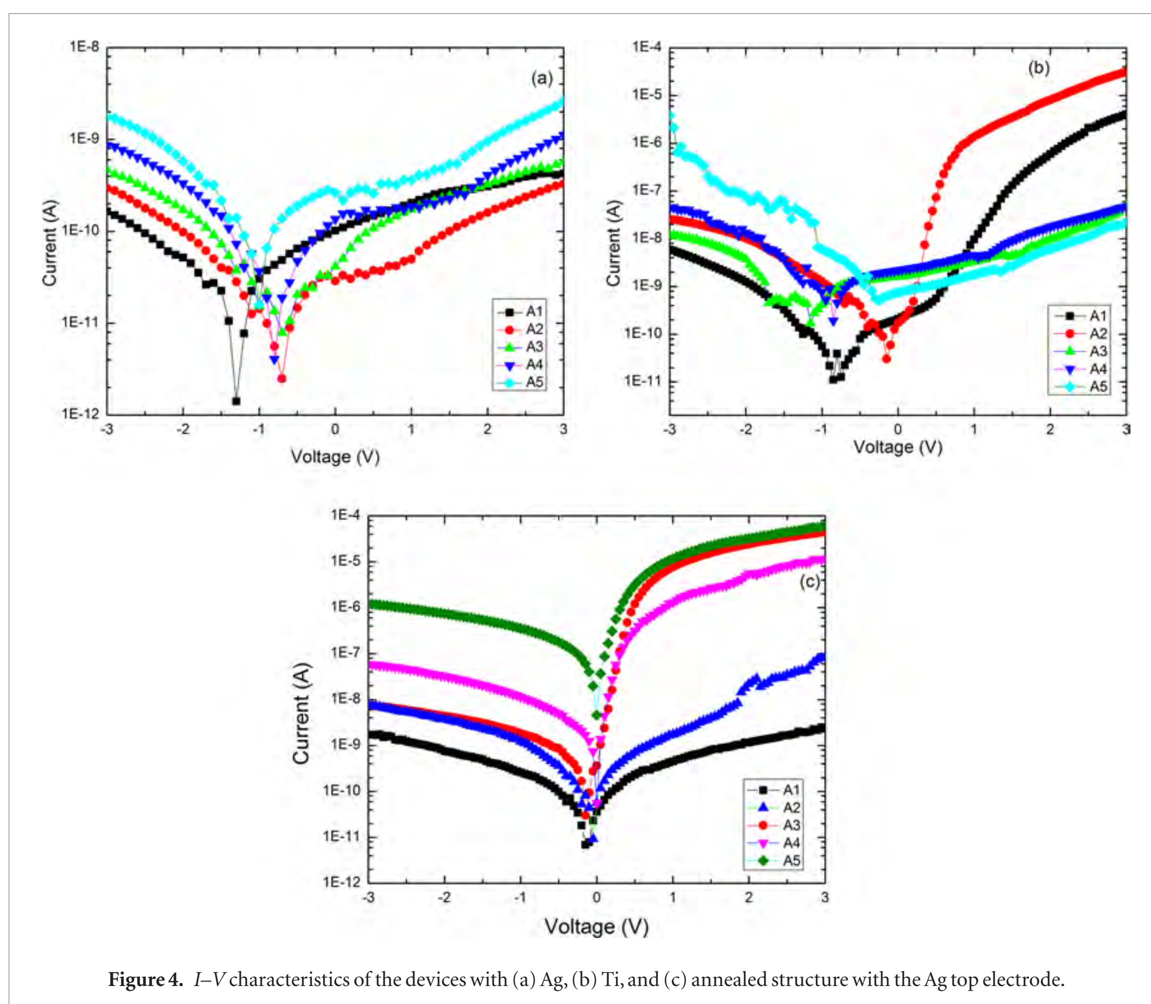

Figure 4. *I–V* characteristics of the devices with (a) Ag, (b) Ti, and (c) annealed structure with the Ag top electrode.

As the area is increased from A2, the current increases and the minimum leakage current is obtained at a smaller negative value. This is due to the larger area to oxygen vacancy ratios thus requiring a smaller negative voltage to inject electrons from the applied field in negative biasing as discussed in the *C–V* results. At −3 V, the results are in accordance with the *C–V* results of Ag electrodes. There is no high increase in the leakage current for areas A4 and A5 because the current due to FFE is decreasing. The results show that we can achieve high tunability by using Ag electrodes of size greater than A3 with low leakage current.

With the Ti top electrodes in figure 4(b), the same trend as Ag is observed from the small size areas A1 and A2 and the same explanation applies. For A1, the leakage current decreases as the voltage is reduced from 3 to 0.35 V and then it becomes constant. Some remnants of oxygen vacancies are observed at 0 V. It should be noted that the top and the bottom electrodes are synthesized under the same conditions and the presence of fixed positive charges under the top electrode cannot be ignored [33]. As a negative bias is applied to the top electrode, the oxygen vacancies move towards the top electrode where a fixed positive charge is already present, resulting in smaller leakage current. On applying the positive voltage to the top electrode, the oxygen vacancies travel towards the bottom electrode, resulting in a significant increase of the leakage current. The leakage current becomes small for A3 and then starts to increase by increasing the area. This shows that the electric field intensity decreases by increasing the area, lowering the barrier for injection and no significant increase in leakage current is observed for positive applied voltage. Also, the current due to FFE decreases by increasing the area. The results show that leakage current changes by changing the area, in the same manner as for Ag electrodes but with reduced tunability and capacitances.

After annealing, the sample with the Ag top electrodes (figure 4(c)), shows the *I–V* curve to be symmetrical around 0 V. This can be correlated with the *C–V* diagrams. The *C–V* curves become smooth for A1 and A2 and then nonlinearity starts. As shown in the *I–V* diagram, the curves are symmetrical around 0 V for A1. It is slightly asymmetrical for A2 and the asymmetry increases as the area is increased. The leakage current is again high during positive biasing. That is due to the fixed charges on the bottom electrode playing an important role as discussed earlier. There is no indication of fixed charges under the top electrode due to the different deposition conditions of the both electrodes [33].

4. Conclusion

The nonlinear properties of STO films are studied by varying the area and materials of the top electrode and oxygen vacancies are observed to play a crucial role in the nonlinearity of the device. It is observed that linearity and tunability can be controlled by changing the area and the electrode type. Even the nonlinear *C–V* behavior of the STO can be made linear by altering the density of oxygen vacancies. With respect to the Ag top electrode, the best tunability with reduced leakage current is achieved from A4 (equal to 10 for as-deposited structure) and the quality factor increases after annealing. The Ti electrodes do not show good characteristics as compared to Ag electrodes. The Ti electrodes show smaller capacitance, tunability, as well as quality factor in addition to higher leakage currents.

Acknowledgments

The work was supported by City University of Hong Kong Applied Research Grant (ARG) No. 9667104. One of the author, Mr Saqib Jabbar, is grateful to the Higher Education Commission (HEC) of Pakistan for financial support under IRSIP.

References

[1] Ha S, Lee Y S, Hong Y P, Lee H Y, Ko K H, Kim D W, Hong H B and Hong K S 2005 The effect of substrate heating on the tunability of rf-sputtered Bi_2O_3–ZnO–Nb_2O_5 thin films *Appl. Phys.* A **80** 585
[2] Bahl I 2003 *Lumped Elements for RF and Microwave Circuits* (Boston, MA: Artech House Publishers)
[3] Mortenson K E 1974 *Variable Capacitance Diodes: The operation and Characterization of Varactor, Charge Storage and PIN diodes for RF and Microwave Applications* (Boston, MA: Artech House Publishers)
[4] Subramanyam G *et al* 2013 Challenges and opportunities for multi-functional oxide thin films for voltage tunable radio frequency/microwave components *J. Appl. Phys.* **114** 191301
[5] Tiggelman M P J, Reimann K, Rijs F V, Schmitz J and Heuting R J E 2009 On the trade-off between quality factor in tuning ratio in tunable high-frequency capacitors *IEEE Trans. Electron Devices* **56** 9
[6] Petrova P P and Alford N M 2005 Improved $SrTiO_3$ thin films using oxygen relaxation technique *Appl. Phys. Lett.* **87** 222902
[7] Miao B, Mahapatra R, Wright N and Horsfall A 2008 The role of carbon contamination in voltage linearity in leakage current in high-k metal-insulator-metal capacitors *J. Appl. Phys.* **104** 054510
[8] Ren T L, Wang X N, Liu J S, Zhao H J, Shao T Q, Liu L T and Li Z J 2002 Characteristics of silicon-based $Ba_xSr_{1-x}TiO_3$ thin films prepared by a sol–gel method *J. Appl. Phys.* D **35** 923
[9] Chiang K C, Lin J W, Pan H C, Hsiao C N, Chen W J, Kao H L, Hsieh I J and Chin A 2007 Very high density (44 fF μm^{-2}) $SrTiO_3$ MIM capacitors for RF applications *J. Electrochem. Soc.* **154** 214
[10] Fedorov I, Železný V, Petzelt J, Trepakov V, Jelínek M, Trtík V, Cernanský M and Studnicka V 1998 Far-infrared spectroscopy of a $SrTiO_3$ film *Ferroelectrics* **413** 208
[11] Müller K A and Burkard H 1979 $SrTiO_3$: an intrinsic quantum paraelectric below 4 k *Phys. Rev.* B **19** 3593
[12] Kaynak C B, Lukosius M, Tillack B, Wenger C, Blomberg T and Ruhl G 2011 Single $SrTiO_3$ and $Al_2O_3/SrTiO_3/Al_2O_3$ based MIM capacitors: impact of the bottom electrode material *Microelectron. Eng.* **88** 1521
[13] Marozau I, Shkabko A, Dinescu G, Dobeli M, Lippert T, Logvinovich D, Mallepell M, Weidenkaff A and Wokaun A 2008 RF-plasma assisted pulsed laser deposition of nitrogen-doped $SrTiO_3$ thin films *Appl. Phys.* A **93** 721
[14] Chase D R, Chen L Y and York R A 2005 Modeling the capacitive nonlinearity in Thin-Film BST varactors *IEEE Trans. Microw. Theory Tech.* **53** 10
[15] Yadav S and Ghosh S 2016 Amorphous strontium titanate film as gate dielectric for higher performance and low voltage operation of transparent and flexible organic field effect transistor *ACS Appl. Mater. Interfaces* **8** 10436
[16] Kim D W, Lee J J, Kwon Y S and Cong H S 1996 Characteristics of an area-variable varactor diode *IEEE Trans. Microw. Theory Tech.* **44** 11
[17] Ueno S, Nakashima K, Sakamoto Y and Wada S 2015 Synthesis of silver-strontium titanate hybrid nanoparticles by sol–gel-hydrothermal method *Nanomaterials* **5** 386
[18] Yan X B, Li K, Yin J, Xia Y D, Guo H X, Chen L and Liu Z G 2010 The resistive switching mechanism of Ag/$SrTiO_3$/Pt memory cells *Electrochem. Solid State Lett.* **13** H87
[19] Lee C H *et al* 2013 Exploiting dimensionality and defect mitigation to create tunable microwave dielectrics *Nature* **502** 532
[20] Lukosius M, Kaynak C B, Wenger C, Ruhl G, Rushwoth S and Baumann P 2011 Atomic vapor deposition of Ti–Ta–O thin films for metal-insulator-metal applications *Thin Solid Films* **519** 3831
[21] Bavadi R and Valedbagi R 2012 Physical properties of titanium nitride thin film prepared by DC magnetron sputtering *Mater. Phys. Mech.* **15** 167
[22] Merie V, Pustan M, Negrea G and Birleanu C 2015 Research on titanium nitride thin films by reactive magnetron sputtering for MEMS applications *Appl. Surf. Sci.* **358** 525
[23] Mehran H, Guchuan Z and Yves A P 2007 A new formulation of fringing capacitance and its application to the control of parallel-plate electrostatic micro actuators *Analog Integr. Circuits Signal Process.* **53** 119
[24] Shaw T M, Trolier-McKinstry S and McIntyre P C 2000 The properties of ferroelectric films at small dimensions *Annu. Rev. Mater. Sci.* **30** 263
[25] Wenger C, Lukosius M, Weidner G, Müssig H J, Pasko S and Lohe C 2009 The role of the HfO_2–TiN interface in capacitance–voltage nonlinearity of metal-insulator-metal capacitors *Thin Solid Films* **517** 6334
[26] Lukosius M, Blomberg T, Walczyk D, Ruhl G and Wenger C 2012 Metal-insulator-metal capacitors with ALD grown $SrTiO_3$: influence of Pt electrodes *Mater. Sci. Eng.* **41** 012015

[27] Lee J H, Lin Y C, Chen B H and Tsai C Y 2010 New metal-insulator-metal capacitor based on $SrTiO_3/Al_2O_3/SrTiO_3$ laminate dielectric *Proc. 10th IEEE Int. Conf. Solid-State Integr. Cicuit technol. (ICSICT) (Shanghai, China, 1–4 November 2010)* (Piscataway, NJ: IEEE) pp 1024–26

[28] Ang C and Yu Z 2004 DC electric-field dependence of the dielectric constant in polar dielectrics: multipolarization mechanism model *Phys. Rev.* B **69** 174109

[29] Szot K, Speier W, Bihlmayer G and Waser R 2006 Switching the electrical resistance of individual dislocations in single crystalline $SrTiO_3$ *Nat. Mater.* **5** 312

[30] Scott J F 2006 Nanoferroelectrics: statics and dynamics *J. Phys.: Condens. Matter* **18** R361

[31] Zubko P, Jung D J and Scott J F 2006 Electrical characterization of $PbZr_{0.4}TiO_{0.6}O_3$ capacitors *J. Appl. Phys.* **100** 114113

[32] Paskaleva A, Lemberger M, Bauer A J and Frey L 2011 Implication of oxygen vacancies on current conduction mechanism in TiN/$Zr_{1-x}Al_xO_2$/TiN metal-insulator-metal structures *J. Appl. Phys.* **109** 076101

[33] Mojarad S A, Kwa K S K, Goss J P, Zhou Z, Ponon N K, Appleby D J R, Al-Hamadany R A S and O'Neill A 2012 A comprehensive study on the leakage current mechanisms of Pt/$SrTiO_3$/Pt capacitor *J. Appl. Phys.* **111** 014503

[34] Mojarad S A, Goss J P, Kwa K S K, Zhou Z, Al-Hamadany R A S, Appleby D J R, Ponon N K and O'Neill A 2012 Leakage current asymmetry and resistive switching behavior of $SrTiO_3$ *Appl. Phys. Lett.* **101** 173507